SPECIAL TOPIC • OPEN ACCESS

Tokamak evolution and view to future

OPEN ACCESS
IOP Publishing | International Atomic Energy Agency
Nuclear Fusion
Nucl. Fusion **59** (2019) 015001 (15pp)
https://doi.org/10.1088/1741-4326/aaee92

Special Topic

Tokamak evolution and view to future

S.V. Mirnov[1,2]

[1] JSC 'SSC RF TRINITI', Troitsk Dep. Pushkovih St 12, Moscow, 108 840, Russian Federation
[2] NRU MPEI, Krasnokasarmennaya St., 14, 111250, Moscow, Russian Federation

E-mail: mirnov@triniti.ru and sergeimirnov@yandex.ru

Received 25 August 2018, revised 7 October 2018
Accepted for publication 6 November 2018
Published 13 December 2018

Abstract

The article begins with a brief review of the achievements of Russian tokamaks in the active period of their development from 1962 to 1973, under the leadership of academician L.A. Artsimovich. During these years, the following basic issues were solved: the equilibrium problem, the MHD stability of the plasma column, and creation of the hot plasma with intense DD neutron radiation. It was shown that the ion confinement in tokamaks is close to the neoclassical model, and the electron confinement is abnormal. It improves with the increasing frequency of collisions, the opposite of the case with ions, in what is known as the alternative model of confinement along the magnetic field. Finally, the first scaling law for the energy lifetime of plasma was obtained, which accurately predicted the plasma parameters of the next generation of tokamaks (the so-called T-4 scaling). The subsequent movement in this direction (the 'Artsimovich vector') led to the creation of DT reactors with a fusion power of up to 10 MW (TFTR, JET) and to the ITER project. The main objective of the further development of tokamaks is their transition to steady-state fusion operation, which is a prerequisite for their use in industrial power generation. This makes it necessary to re-evaluate the achievements and obstacles that have to be overcome. The first limitation which thus arises is the so-called P_H/S limit, which limits the value of the plasma heating power in a tokamak, as well as the discharge duration Δt (the 'TRIAM vector') in current tokamaks ($\Delta t \sim 1/(P_H/S)^{1.7}$). Analysis of the existing experimental data shows that the most probable reason for the limitation of P_H in existing tokamaks is the breakdown of the plasma sheath in the places of direct contact of the plasma with the wall. The reason for limiting the discharge duration Δt may be the gradual accumulation of the erosion products in the contact zones of the plasma with the tokamak first wall, which can facilitate such a breakdown. Creating a closed circulating lithium flow between the first wall and plasma is proposed as the solution to the problem of accumulation of the products of the first wall erosion. Preliminary studies (appendices A and B) have shown that the undesirable accumulation of tritium in the protective lithium films can be avoided if the temperature of the wall of the tokamak discharge chamber does not exceed 400 °C.

Keywords: tokamak, steady-state, tokamak limits, liquid lithium

(Some figures may appear in colour only in the online journal)

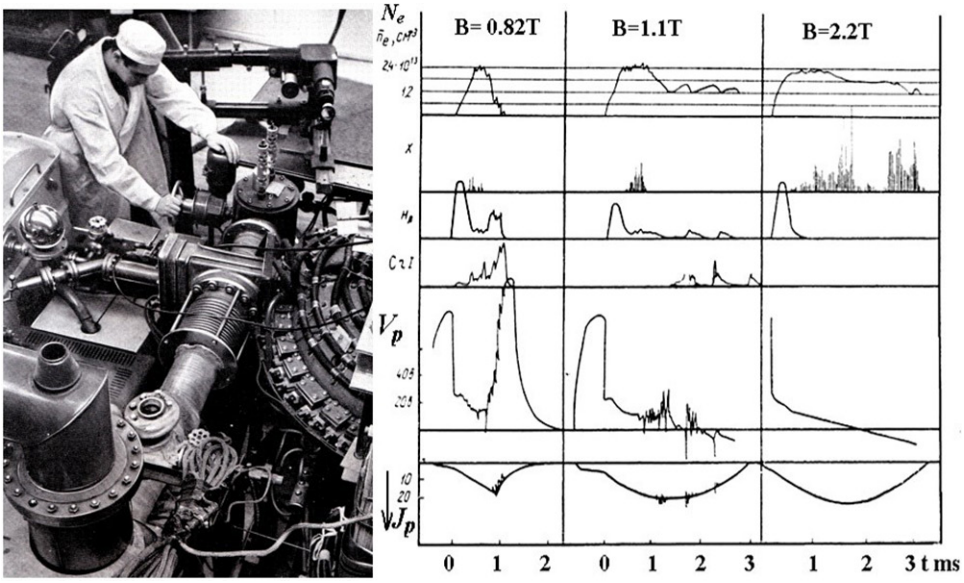

Figure 1. View of TM-2 (left) and right: waveforms of main parameters of TM-2 for three shots with different toroidal magnetic field B [1].

1. Introduction: achievements of Russian tokamaks

The Russian (Soviet) program of fusion investigations began with Stalin's decree in 1951, more than 66 years ago. However, it took 10 years, until the winter of 1961–62, before E.P. Gorbunov and K.A. Razumova, in the Kurchatov Institute in Moscow, had their first success [1]. On tokamak TM-2, they obtained an unusual 'macroscopically stable' discharge without deep 'grassy' oscillations of the waveforms of the main plasma parameters. That was a 20 kA hydrogen shot of a few milliseconds duration (Δt) and with a plasma temperature of up to 100 eV (~10^6 K!), which was something of a sensation for the plasma researchers of those times.

Figure 1 [1] presents a view of the TM-2 tokamak and a series of waveforms of the TM-2 plasma parameters: the electron density $N_e(t)$, the hard x-ray intensity X, the spectral line $H_\beta(t)$ as the indicator of plasma interaction with the tokamak limiter, the intensity of *Cr*- spectral lines as the indicator of plasma interaction with the chrome-nickel vacuum chamber, the loop voltage $V(t)$ as the indicator of magnetic perturbations at the edge of the plasma column, and the discharge current $J_p(t)$ for three hydrogen discharges obtained with different toroidal magnetic fields $B = 0.8$ T, 1.1 T and 2.2 T. The 'smooth' behavior of $V(t)$ and the almost constant $N_e(t)$ in the last case of $B = 2.2$ T were the greatest surprise for plasma physicists.

As we can see, in the TM-2 shot with the magnetic field of 2.2 T, the plasma density was almost constant during the discharge, as many enthusiasts of fusion had dreamed about at that time. These TM-2 discharge regimes looked to be a strange exception to the rules. However, one year later, the same modes of 'smooth' tokamak regimes were obtained in the new large Russian tokamak T-3 [2]. The total current J_p was increased in T-3 up to 40 kA, and the shot duration Δt reached 10 ms. Apart from this, the safety factor $q(a)$ was decreased from 8 in the 'smooth' regimes of TM-2 down to 6. From this moment on, one could speak about a principally new type of macroscopically stable mode of tokamak operation.

The duration Δt of discharges of this type was substantially longer (up to five times) than the estimated value of the plasma energy confinement time τ_E. (The plasma temperature was estimated in both tokamaks through the Spitzer electric conductivity with the assumption of $Z = 1$.) This result ($\Delta t/\tau_E > 5$) was interpreted as an indicator of the quasi-stationary character of the new tokamak discharges. Active investigations of such quasi-stationary tokamak discharges then started, and they continue up to now. What are the main results of this activity and what are the prospects as we see them today?

The main vector of further tokamak studies (the '*Artsimovich vector*'), which were carried out in the Division of Plasma Research of the Kurchatov Institute headed by academician Artsimovich, was directed towards optimization of these new discharge regimes and understanding their nature. In particular, it was directed towards the study of: plasma equilibrium [3, 4], the plasma current and density limits [5–10], and the plasma confinement evolution as a function of the plasma parameters [11–15]. Special attention was given to the development of new methods of tokamak chamber conditioning and to the optimal choice of materials of the plasma-facing components (PFCs).

Figure 2 shows one of the final results of the 1961–71 'Russian tokamaks' activity: the waveforms of the main parameters of a deuterium (DD) discharge in the T-4 tokamak (1971; [13]), accompanied by a pulse of the soft x-ray radiation from the plasma center corresponding to an electron temperature of up to 2.5 ± 0.5 keV and a pulse of the DD neutron yield corresponding to a Dayton temperature of up to 0.6–0.7 keV. (The T-4 tokamak was a development of the T-3 tokamak optimized towards increasing the toroidal magnetic field B_T from 3 T to 4.5 T, and increasing J_p up to 200 kA with $q(a) \approx 2.5$.) That was the initial step of a transition from tokamak laboratory experiments to the investigation of a fusion neutron source (FNS) based on tokamaks.

Together with obtaining the first fusion neutrons, a first scaling law for the energy confinement was produced in these

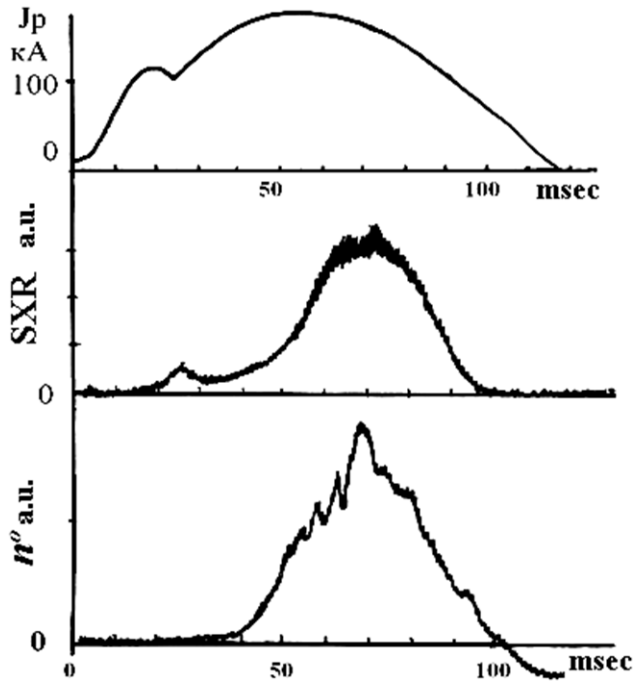

Figure 2. Tokamak T-4 shot (1971 [13]). $B_T = 4.5$ T, $T_e \sim 3$ keV, $T_i \sim 0.7$ keV, DD plasma ($\Delta t/\tau_E > 10$).

years in the Artsimovich Division. By comparing the plasma confinement data obtained on TM-2 (TM-3) and T-3, a scaling law was found for τ_E in Ohmically-heated tokamaks. It was first mentioned in [11] as $\tau_E \sim aJ_p n^\alpha$, where $\alpha \approx 0.3$, and later and more thoroughly in [14, 15]):

$$\tau_E \sim 1.5 \times 10^{-8} B_p \langle n_e \rangle^{0.5} a^2 \text{ s } (B \text{ in Gauss}, \langle n_e \rangle \text{ in } 10^{13}\text{cm}^{-3}, a \text{ in cm}). \quad (1)$$

Besides giving precise predictions of the absolute τ_E values for the next generation of tokamaks (T-10, PLT (Princeton Large Torus)), this scaling gave an indication of the anomalous losses of electron energy along the magnetic field in tokamaks. The positive factor $\alpha > 0$ (confirmed later by ITER τ_E-scaling [16] with $\alpha = 0.4$) meant an unexpected improvement of plasma confinement in tokamaks with an increase of the collision frequency. Kadomtsev, Pogutse and Callen later explained this paradox for closed magnetic configurations in the framework of concepts of the 'braided magnetic field' [15, 17] or 'magnetic flutter' [18].

Figure 3 [19] presents the temporary evolution of the power of neutron yield as obtained in worldwide tokamak investigations during the 25 years following 1971.

Three trends of this evolution seem to be the most important. The first was the progressive increase of tokamak dimensions with a parallel increase of the plasma heating power P_H (up to almost two orders of magnitude) with the multiplication of the total magnetic energy. The second trend was the transition from the traditional tokamak with a circular cross-section to a more progressive, elongated plasma configuration with the poloidal magnetic divertors (ITER-like configuration) first suggested by Artsimovich and Shafranov in 1972 ('Tokamak with non-round section of the plasma loop' [20]).

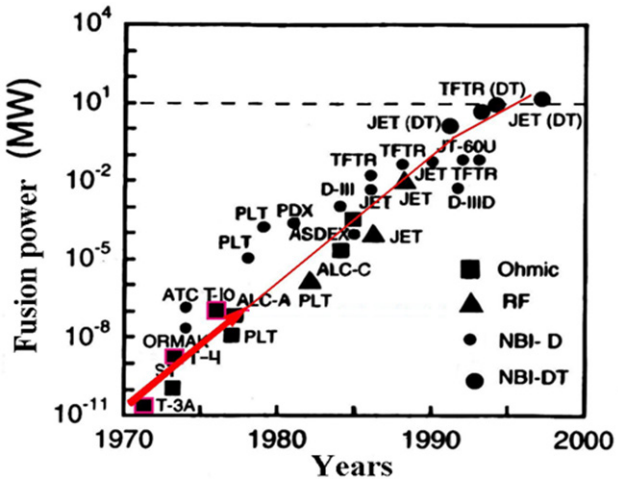

Figure 3. Temporal dynamics of fusion power output in high performance shots of tokamaks (PPPL [19]), arrow–'*Artsimovich vector*' [11] from T-3 to T-10.

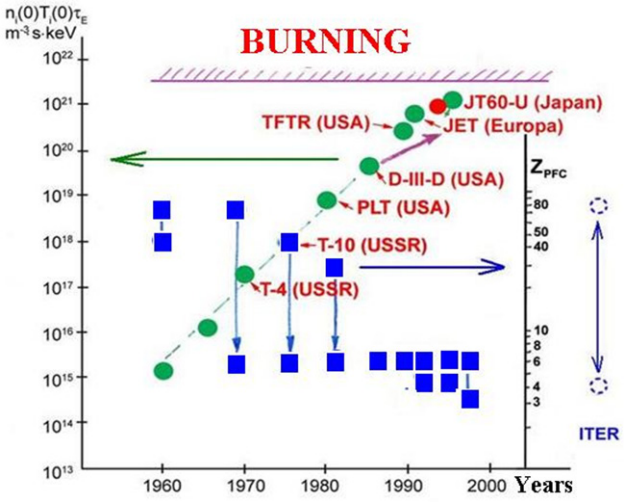

Figure 4. Temporal dynamics of the triple product (circles) and development of PFC materials (squares).

The third tokamak trend was the gradual transition from high-Z materials (SS, Mo, W) as the coating material of the PFC—limiters, first wall, and divertors– to materials with low Z (C, B, Be, Li) during these years. This transition occurred under the hard pressure of experimental facts and in the face of hard resistance from engineers who preferred the refractory metals to graphite, beryllium and lithium. The transition to low-Z materials as the PFC coating was the most important component in the success of the tokamaks in the 1970–90 period.

Figure 4 illustrates the temporal dynamics of the development of the PFC of major operating tokamaks from high-Z to low-Z materials (squares, right axis) along the growth of the triple product $nT\tau_E$ (circles, left axis). The dotted line on the right presents the future PFC materials of ITER.

In particular, Artsimovich was the first author of the idea of using materials with a low Z (graphite or BeO) for the limiters of the Russian tokamaks. A graphite limiter doped with 15% boron (USB-15) was first successfully realized in 1977

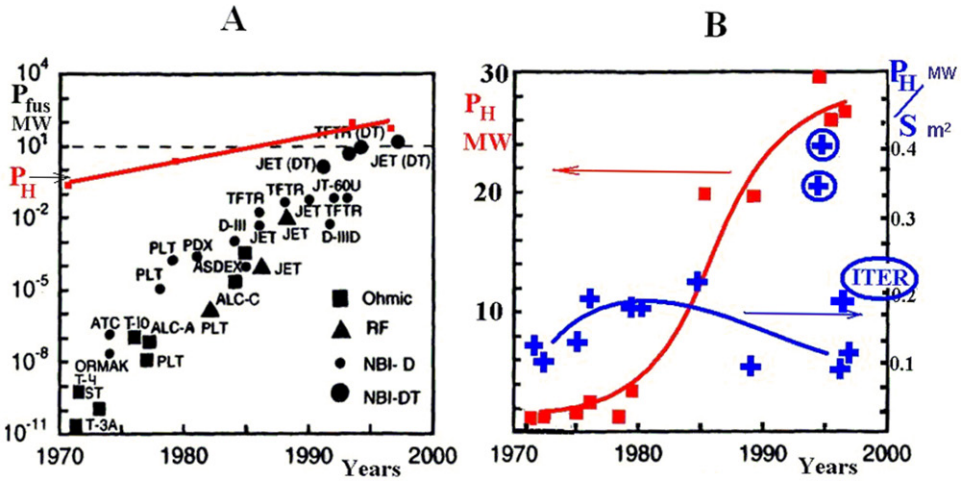

Figure 5. (*A*) The dynamics of neutron production: P_{fus} and P_H. (*B*) P_H (squares) on linear scale, crosses—$q_T = P_H/S$. Adapted from [25].

on the T-4 [21] tokamak—unfortunately, after Artsimovich's death. With these experiments, 'the graphite era in Russian tokamaks' started. After the famous PLT results (1978 [22]) it transformed into 'the world graphite era'.

What are the key recommendations for the future, which we see as the results of almost 60 years of tokamak evolution?

2. The path to future tokamak applications

The most important matter is the knowledge of '*tokamak limits*'. Their summaries (ITER Physics Basis [16]) form the concept of ITER. The most productive method of the searches of '*tokamak limits*' was a comparative analysis of the plasma activity of tokamaks, significantly different in their geometric and energy parameters. For example, the first bright application of this method was to obtain the scaling of the plasma density limit in tokamaks (the '*Murakami limit*'). Already, from the early experiments on tokamak T-3 [2], it was known that the value of the maximum achievable plasma density depends heavily on the quality of conditioning of the tokamak chamber. An additional injection of *Kr* in the plasma column of T-3 decreased the permissible density limit [8]. It was clear to see that an increase in the radiation power of the plasma periphery excited the magnetic activity of the plasma boundary finished by disruptions. The first scaling of the density limit on T-3 (1971Y, $n_{emax} \sim (B_T J_p)^{1/2}$ [7]) showed that it increases with the growth of the magnetic field B_T and the total discharge current J_p, which indicated its cause: the MHD destabilization of the plasma boundary under its cooling by the impurity radiation [7, 8].

However, these results seemed to be particular characteristics of only the T-3 plasma, until 1976, when Murakami *et al.* [23] did not find a universal expression for the maximum achievable density in tokamaks $n_{emax} \sim B_T/R \sim q(a)J_p/a^2$ (the so-called '*Murakami limit*'), which was received after analysis of a sufficiently representative group of tokamaks that were operating in the world at the time. Further activity in this direction resulted, in 1986, in a more comfortable recording of this criterion by Greenwald *et al.* as $n_{emax} \sim J_p/a^2$; the so-called '*Greenwald limit*' [24], allowing it to be used in a wider range of J_p. This method of comparative analysis of finding '*tokamak limits*' from a particular case to a common case will be used in this paper.

All ITER '*tokamak limits*' searches (J_p, n_{emax}, β-limits) were based on the rich experience of numerous quasi-stationary tokamaks with shot durations of only 5–10 times the energy confinement time τ_E of the plasma. However, the idea of industrial use of a tokamak as a steady-state fusion reactor demands additional knowledge about the role of the long-term effects of plasma behavior and, firstly, about the 'permissible' level of plasma heating (P_H), which finally restricts the obtaining of high plasma pressure and neutron output in a tokamak. It demands analysis of the '*limits problem*' again.

The first subject of such an analysis should be the 'P_H/S limit' [25] for the so-called 'high performance tokamak regimes', where P_H is the total heating power of plasma, which should be equal to the total energy losses in the quasi-steady-state tokamaks, and S is the inner area of the tokamak chamber facing the plasma. The 'high performance tokamak regimes' are the best tokamak shots, with the maximum plasma energy and duration.

2.1. Phenomenology of P_H/S limit

Figure 5(*A*) presents the above-mentioned temporal dynamics of the neutron yield (figure 3) for a number of well-known tokamaks, but with the addition of a solid line showing the dynamics of the plasma heating power P_H used in those 'high performance' experiments. Figure 5(*B*) shows the same P_H dynamics, but on a linear scale. As one can see, within a period of 25 years, the interval of P_H used in the high performance tokamak regimes multiplied roughly 60 times, while the neutron output increased by 12 orders of magnitude. However, if we divide these well-measured values of P_H by S, we find a very clear result (figure 5(*B*), crosses). The value of the specific energy load $q = P_H/S$ in all these tokamaks remained approximately constant ($\approx 0.2 \pm 0.1$ MW m^{-2}) throughout the 25 years of high performance tokamak operation,

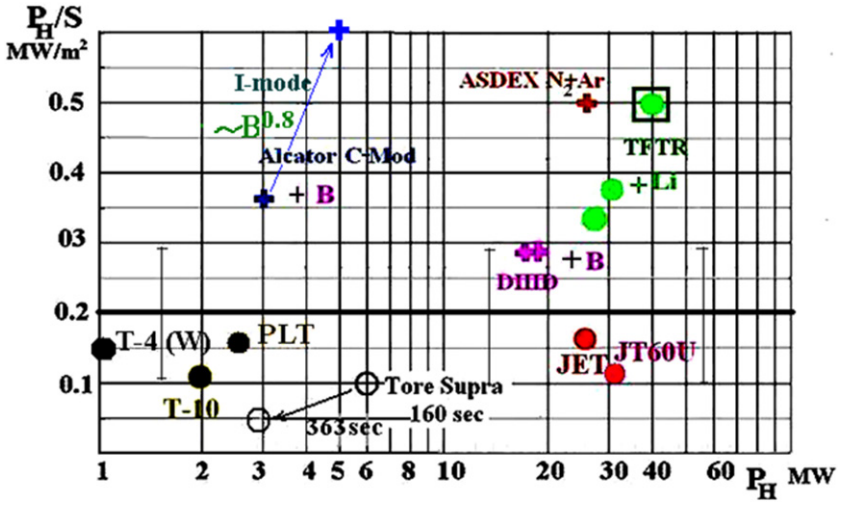

Figure 6. P_H/S as a function of P_H for the 'high performance shots' from several known tokamaks: TFTR [26, 27], JET [31], JT-60U [28], PLT [24], T-4 [13], ASDEX –U [30], Alcator C-Mod [31], DIIID [32], T-10 [33], and Tore Supra [34].

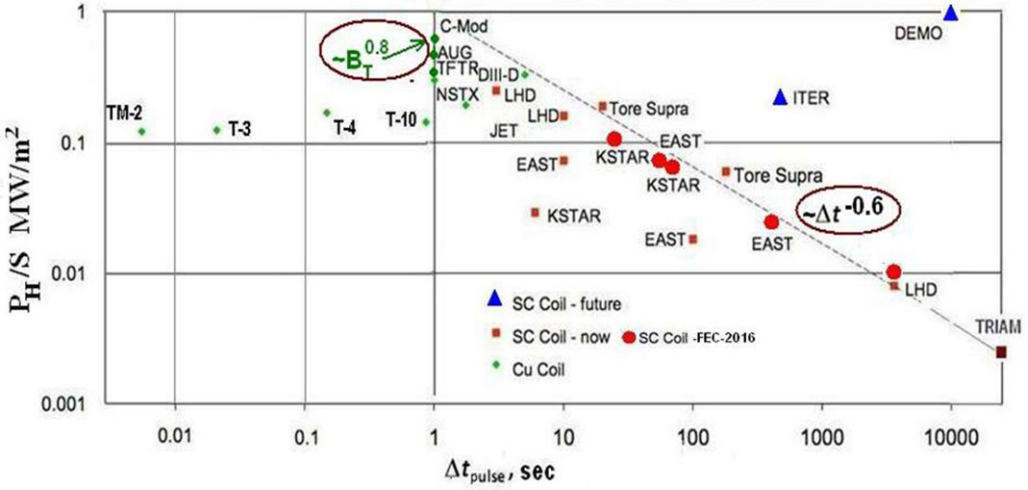

Figure 7. Diagram of P_H/S-Δt. Δt presents the maximum duration of discharge shots obtained in different tokamaks under given values of P_H/S.

despite different methods of plasma organization and heating being employed [25]. (Note that for ITER, the value of $P_H/S = 0.2$ MW m^{-2} was suggested [16], which is close to this limit.) The attempts to overcome this limit are represented in figure 5(*B*) by two points where $P_H/S \approx 0.4$ MW m^{-2} (they are encircled), which were achieved in TFTR experiments [26, 27] and ended with disruptions.

As the next step, figure 6 presents the achievable ('permissible') P_H/S values together with P_H ('P_H/S-P_H *diagram*') for the 'high-performance shots' on a number of tokamaks [26–34]. They differ significantly in size, and in the toroidal magnetic field (up to 8 T in Alcator C [31]), and in the high-Z versus low-Z coating of PFC. One example of successful cooling of the plasma periphery by $N_2 + Ar$ injection (ASDEX-U [30]) is also shown. One can see that the real achieved 'permissible' values of P_H/S for the major part of the tokamaks are concentrated around 0.2 ± 0.1 MW m^{-2}. This means that we can again speak about some kind of a soft P_H/S limit. As an example of the almost successful overcoming of this limit, figure 6 presents the TFTR shot with $P_H/S \approx 0.5$ MW m^{-2} (in the rectangle) [27], which was obtained with an 'excess' of P_H (40 MW), over the 'permissible' level (~30 MW). Unfortunately, this shot also ended with a minor disruption.

However, this figure clearly shows significant deviations of achievable values of P_H/S from the 0.2 MW m^{-2} level. Let us try to determine the reason for these deviations. First, note that the points corresponding to the tokamaks with low-Z coatings of the first wall generally correspond to the values of P_H/S higher than 0.2 MW m^{-2}. Secondly, the high values of $P_H/S \approx 0.6$ MW m^{-2} were achieved on ASDEX-U, when the impurities ($N_2 + Ar$ puffing) cooled the plasma periphery, and the direct contact between the plasma and the wall was therefore deliberately weakened. The high values of P_H/S were also obtained on the Alcator C tokamak, which has the highest toroidal magnetic field, of up to 8 T. (In the other tokamaks considered here, with the exception of TFTR, B_T was within the range of 2–3 T.) As was shown [31]. On Alcator C the 'permissible' P_H increases with B_T at degree 0.8 roughly (i-mode). Finally, the superconductive tokamak Torus Supra, which had

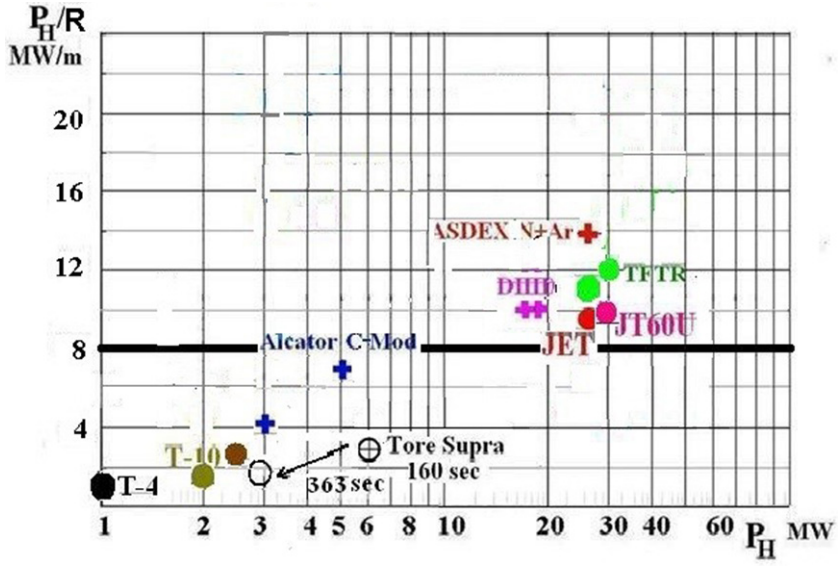

Figure 8. Diagram of $P_H/R - P_H$ for the tokamaks mentioned in figure 6.

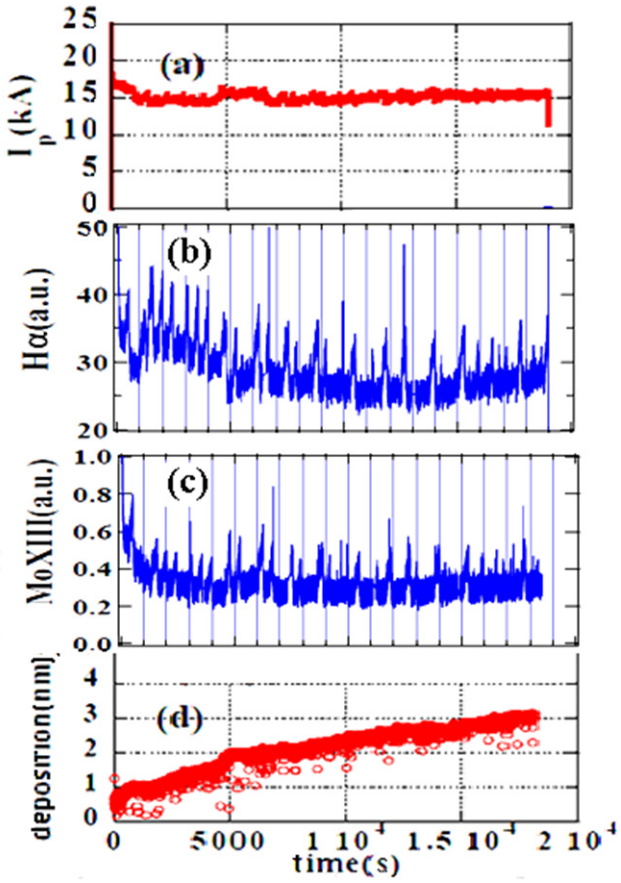

Figure 9. Waveforms of important operating parameters: plasma current, H_α and *MoXIII* intensities, and thickness of the PFC deposition during the record discharge shot of TRIAM-1M tokamak [36]. Adapted courtesy of IAEA. Figure from [36]. Copyright 2005 IAEA.

the highest discharge duration among the current tokamaks, of up to $\Delta t \sim 160$–300 s, was operated only at low values of P_H/S (in range 0.1–0.05 MW m^{-2}) and shows a clear trend of Δt reduction along with increasing P_H/S.

To clear up this trend of Δt reduction along with increasing P_H/S, the author presents figure 7 with a diagram of P_H/S-Δt following [35], where Δt was presented as the maximum duration of discharge pulses obtained in different tokamaks under given values of P_H/S. Unlike [35], the author has included in the P_H/S-Δt diagram only the high performance regimes of all the above-mentioned tokamaks, as well as old known results published by the TRIAM–M1 tokamak group [36] and TM-2 [1], together with some new tokamak results, presented at the 26 FEC conference of the IAEA (Kyoto, 2016) [31, 37, 38, 39]. As we can see in figure 3, in a wide range of variation of Δt from 1 ms up to 10–20 s, the P_H/S parameter looks almost constant (quasi steady-state regime) as we have seen above, at around 0.2 ± 0.1 MW m^{-2}, but then progressively decreases up to the TRIAM record of 20 000 s [36] by following the simple equation (the '*TRIAM vector*'):

$$P_H/S(\mathrm{MW\,m^{-2}}) \approx 1/\Delta t^{0.6}\,(\mathrm{s})\,, \text{ or} \tag{2}$$

$$\Delta t \approx 1/(P_H/S)^{1.7}\ \mathrm{s}\,. \tag{3}$$

If we count this restriction as being fair for all 'high performance quasi steady-state tokamaks' with $P_H/S = 0.2 \pm 0.1$ MW m^{-2} limit, the allowed duration of their discharge shots Δt should be limited to 50 s only. How does it overcome this limitation, which can be critical for the industrial applications of a tokamak?

What physical processes can be the basis constraint P_H?

3. Discussion

The first question that we must ask ourselves is as follows: are we sure that the surface area S (~Ra) of the discharge chamber facing the plasma (rather than its volume V (~Ra^2) or its linear size (e.g. R)) defines the geometric factor of the invariant? Note that the R scaling is sometimes popular in computer simulations of virtual tokamak reactors with a magnetic geometry similar to ITER. In such cases, R is used in the invariant form P_H/R. What happens if we try to spread this invariant

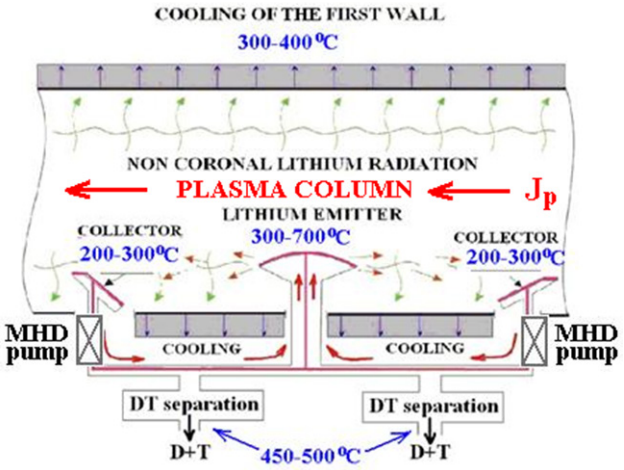

Figure 10. Schematic diagram of the Li and DT circulation loop in a steady-state tokamak FNS [52].

for all tokamaks? Figure 8 presents the $P_H/R - P_H$ diagram for the tokamaks mentioned in figure 6. One can see that the P_H/R ratio grows monotonically with P_H about 10 times as P_H increases approximately 30 times, in contrast to the slight scatter in the P_H/S ratio. Thus, the P_H/S ratio may not claim the role of an invariant across tokamaks of all sizes and P_H values. However, for a narrow areal of tokamaks with poloidal divertors and minor radii of $a = 0.5$–1 m, this ratio remains nearly constant, which justifies its use for the purposes of computer simulation. Finally, a similar diagram $P_H/V - P_H$ shows too high a scatter in the data, which obviously excludes the possibility of using this ratio as an invariant for any appreciable group of tokamaks. Thus, the proportional increase in the allowed values of P_H from S should be interpreted as a fundamental feature of the P_H limits.

Can we explain the existence of this limit within the framework of the known physical laws describing the behavior of plasma in tokamaks? A breakdown of the plasma sheath between the plasma boundary and the wall coated by the deposits of the erosion product of PFC can be suggested as an explanation of the physical nature of this limit [39].

3.1. Breakdown of the plasma sheet as a probable origin of the P_H/S limit

The growth of the upper boundary of this limit with gas puffing in the scrape-off layer (SOL) between the chamber wall and the hot plasma boundary [30], and its growth in the case of a low-Z coating of the tokamak first wall [26, 27, 32], force us to assume that the main physical reason for this limit is direct plasma–wall contact. Its negative consequences are usually usually by an increase of radiation cooling of the plasma periphery by gas puffing and low-Z injection.

The most negative consequence of direct plasma–wall interaction is the breakdown of the plasma sheath between the plasma and the tokamak first wall, with the formation of unipolar arcs (e.g. see [40]) and a rich emission of the wall erosion products into the hot plasma column. The next candidate for causing plasma pollution by the erosion materials is the vacuum breakdown (e.g. see [41]) of the plasma sheath. The reasons and consequences are similar in the two cases. They are the too-high electric field E on the solid surface and the influx of the erosion material, which can interrupt tokamak operation.

The reason for the excitation of the electric field E on the solid surface of the wall is the electric potential of the sheath ($\sim 3T_e$) between the plasma and the wall. It reduces the electron heat flux and maintains the ambipolar plasma flux onto the wall, which is proportional to the mean electron pressure P_e near the place of the plasma–wall contact [40]. If we take into account that the width of the potential sheath should have a scale of the Debye length, then the electric field E near the first wall of a tokamak and in the region of contact with the plasma should be proportional to $(n_e T_e)^{1/2} \sim P_e^{1/2}$. If E is limited by the breakdown voltage of the sheath (E_C), then it will limit the permissible local energy flux from the plasma column onto the wall without the too-high influx of erosion material. As a result, this will limit the total energy flux $\sim P_H/S$ from the hot plasma column without radiation losses and energy heat flow onto the divertor.

Taking into account the typical parameters of the peripheral plasma in a 'regular' tokamak discharge, it is possible to estimate the order of magnitude of the electric field E at the plasma–wall boundary. For the values of plasma density near the wall of (3–5) $\times 10^{18}$ m^{-3} and $T_e = 30$ eV, typical of current tokamaks, the value of E at the place of the plasma–wall contact will be about 5×10^6 V m^{-1}, which is within the range of vacuum breakdown, $E_C \sim 10^6$–10^8 V m^{-1} [41].

One common opinion is that most of the energy flux derived from the plasma during 'regular' tokamak shots should be directed to the divertor or limiter, and only a small part in the form of radiation falls onto the wall, thereby restricting P_e near the wall to a vanishingly small level. However, as is known from practice with real tokamaks, a significant part of the surface of the plasma column (no less than 20%–30%) directly contacts the chamber wall in particular, due to the destruction of magnetic surfaces during the development of various types of peripheral turbulence, and in spite of the use of various kinds of limiters or divertors. These areas probably determine the 'permissible' limit of P_H/S in each real tokamak. We can assume that the relatively high variation of the 'permissible' P_H/S from 0.1 to 0.3 MW m^{-2} (figure 5) reflects different roles that these 'areas of direct interaction of the plasma with the wall' play in various tokamaks, with different levels of radiation losses and energy streams onto divertors. Let us make a simple estimation and write the critical heat load on the area of a direct plasma–wall contact before breakdown in the form of P_C/S. Then, the value of P_C is equal to $P_H - P_\Sigma$, where P_Σ is the total power flux from the hot plasma by radiation and plasma energy stream onto the divertor. Its fraction is from 0.1 to 0.7 (± 0.1) of P_H in real tokamaks. Therefore, we have $P_C = P_H(1 - K)$, where K can vary from 0.1 to 0.7. Accordingly, the permissible value of P_H/S will vary up to three times at a fixed P_C. This is very close to the observed data scatter in figure 6.

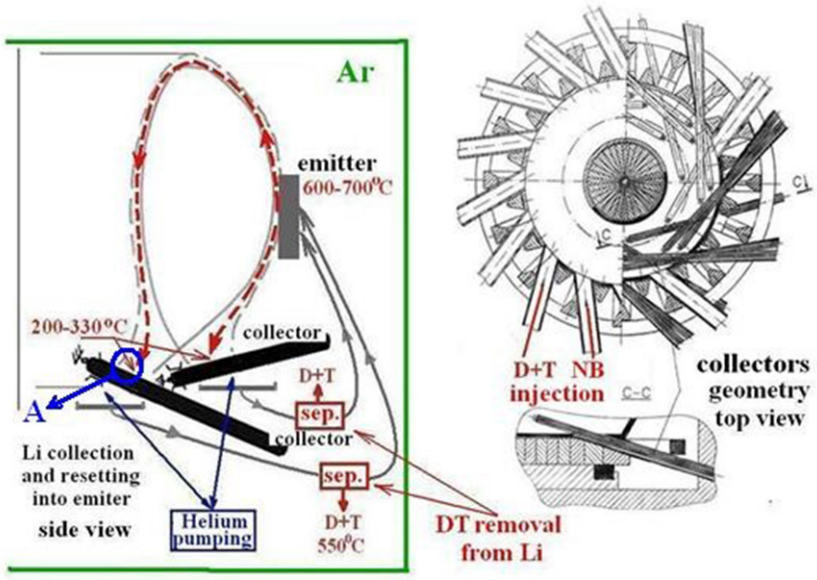

Figure 11. On the left: Li circulation loop for a steady-state FNS: (A) region of the most probable Li collection; (Ar) shell coating tokamak to prevent lithium from poisoning by accidental air contacts. The arrows show the directions of drift of Li ions in the divertor SOL. On the right: top view of the FNS tokamak with longitudinal (tangent to B_T) rod-type divertor targets. Reproduced from [47].

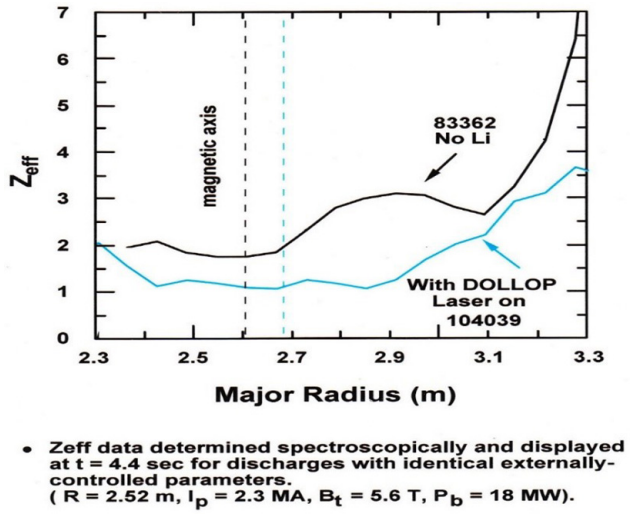

Figure 12. Radial distribution of $Z_{\text{eff}}(R)$ for two DD shots without and with Li injection by laser evaporation in TFTR [44]. Reproduced with permission from D. Mansfield.

3.2. Tokamak as an analog of an ion (getter) pump

What physical mechanism can restrain the shortening of the quasi-stationary discharge with the growth of the P_H/S parameter? At first glance, this may be a result of the gradual accumulation of the PFC erosion products in the tokamak chamber during the long-duration interaction of the plasma with the wall. It is well known that a similar effect takes place during long-term operation of the so-called 'ion (getter) pumps'. These are electric discharge pumps with titanium electrodes, whose spraying provides the capture of ionized gases by titanium films, which are products of the electrode discharge. However, ion pumps fail over time and require periodic restoration by electric discharges, transferring the gas-saturated films from the active to the passive elements of the pump. One can conduct a direct parallel between the long-term activity of a tokamak with PFC erosion and the operation of ion pumps.

The main objective of the primary conditioning of the tokamak first wall is the removal of the impurity films from the plasma-facing surfaces by using different types of plasma discharges. It is well known that the presence of organic or oxide films on the surface of a tokamak chamber leads to an intense development of unipolar arcs. Their breakdown voltage increases and the arc frequency reduces as the film thickness on the contact surface decreases. It is also known that the tokamak conditioning is finished when the influence of arcs can be neglected in the course of routine tokamak operation with moderate P_H/S. It is obvious to suppose that metal films saturated by plasma gases in the ion pumps and tokamaks should behave analogously to organic and oxide films as their thickness decreases or increases.

Sometimes, cleaning by a glow discharge can be used between a tokamak's regular shots, with the aim of improving their reproducibility. The erosion products of active PFCs should accumulate on the surface of passive PFCs and the tokamak chamber wall (redeposition) during long-term plasma operation. It is obvious that this process should increase nonlinearly with increasing P_H. This is opposite to the discharge cleaning of the first wall. It should be taken into account that the thickening of all deposited films (whether organic or metal) should finish with the loss of thermal contact with the substrate, which can be an origin of their overheating during a plasma shot. This means that long-term plasma operation promotes an increase in the probability of the arcs' excitation and cathode spot formation on the formerly passive PFC by analogy with ion pumps. The visible signs of arc craters on the PFCs and first wall can be observed after long-term tokamak operation.

Such an analogy (model) of an 'ion pump' allows us to understand the mechanism of the limiting of tokamak pulse duration ($\Delta t \approx 1/(P_H/S)^{1.7}$ s, the so-called 'TRIAM vector' (3)) during quasi-steady tokamak operation, as a result of the gradual accumulation of the erosion products on the surface of the tokamak chamber. The well-known TRIAM-1M [36] results qualitatively confirm this concept. Figure 9 from [36] presents waveforms of several plasma parameters during the record discharge shot (pulse) of TRIAM-1M, with a duration of up to 5 h, finished with a disruption: toroidal current $J_p = 15$ kA (maintained by LH current drive), intensities of the H_α and MoXIII spectral lines as indicators of the plasma–wall interaction, and thickness of the erosion products deposited on the wall in the course of the plasma discharge.

As we can see, this superlong plasma discharge was accompanied by two kinds of 'grassy' oscillations: in general, small and frequent spikes, but sometimes (at intervals of approximately 1000 s) high local 'explosions' of deposited films (Mo and H). Both types of oscillations clearly illustrate the 'ion pump' model.

3.3. Ways of making steady-state tokamaks

The first method of making steady-state tokamaks is the radiative cooling of the plasma periphery (SOL) by impurity injection, increasing the P_Σ/P_H ratio to almost 1, as was demonstrated for example in the ASDEX-U experiments [19]. However, active injection of impurities into the SOL (up to $P_\Sigma/P_H \approx 1$) can initiate MARFE excitation and tokamak disruptions. Further, the tendency of impurities in the neoclassical penetration into the plasma core will complicate the current drive problem. This problem is usually considered to be the main obstacle to the creation of a steady-state tokamak. It has attracted the attention of a large part of the fusion community and significant progress has been made in this field. For example, in experiments on DIIID [32], it was possible to obtain a non-ohmic current of 1 MA scale for a period of several seconds. However, these attempts often met seemingly inexplicable difficulties (for example, TRIAM-1M, figure 7), which was clearly associated with too high a parameter P_H/S. This allows us to set the problem of current drive as the next item after the P_H/S limit. Obviously, to facilitate its solution, it is necessary to maintain $Z_{eff}(0)$ at a minimum level.

The second method assumes the simultaneous on-line removal of the PFC erosion products and the 'excess' fuel (D, T) from the tokamak chamber during the operating cycle of the reactor by using of liquid metals. The use of liquid lithium seems the most promising. It can be used as a PFC protector with good transportability in the relatively broad temperature range $T_{melt} = 180$ °C–700 °C [42]. This can provide, in principle, the possibility of creating closed Li circulation as a product of PFC erosion with the trapped fuel (D, T) [43]. A small nuclear charge ($Z = 3$) promotes good compatibility of Li with the hot tokamak plasma, as was shown early in TFTR [44] and in the later tokamak experiments [45, 46]. The injection of Li spray in the SOL plasma demonstrated its poor penetration into the plasma core as an impurity in many experiments [44–46]. The emissivity of Li in the SOL can be increased by using the so-called 'noncoronal regime' of light emission (intense radiation of Li ions until they reach the coronal equilibrium in the SOL; see appendix A [43]). This second method seems more radical and is also more complicated.

Today, two proposals are being discussed to remove the products of erosion of the first wall from the tokamak chamber during steady-state operation with the use of liquid lithium.

The first one [43, 47] is intended to provide steady-state operation of a FNS on a tokamak basis with a lithium coating of the chamber wall. (The FNS is an intermediate step between the laboratory fusion device and self-sustaining DT reactors with ignition. The task of an FNS is the production of intense fluxes of fast neutrons to meet the needs of LWR nuclear power, in particular, for the burning of minor actinides (the ashes of LWR) or production of fuels (^{233}U, ^{239}Pu) from weakly active ^{238}U and ^{232}Th for the same LWR. Prototypes of FNSs could be the TFTR and JET DT tokamaks).

The second proposal provides steady-state operation of a pure DT tokamak reactor with a temperature of the first wall of at least 700 °C. This excludes the possibility of wall protection by any type of lithium coating. Liquid lithium in this case is supposed to be used as a free jet in the divertor with a flow rate of 100 l s^{-1} and more, which is close in order of magnitude to the flow rate in the lithium jet of the neutron source IFMIF. First of all, such a liquid lithium jet is intended [48] to serve as the heat receiver of the tokamak divertor. The second aim of this lithium jet is to remove the particle flow of the 'excessive fuel' (D, T). Simultaneously, the products of erosion of the chamber wall will be captured and removed. The products of erosion can then be removed from the liquid lithium by using a special filter placed outside the chamber. The 'excessive fuel' can be separated from the liquid lithium by various technological methods and can be sent back to the fuel injection system.

The first practical use of lithium films flowing close to the tokamak first wall was implemented on the EAST tokamak [49]. It is expected that such an important direction of tokamak research will continue for some years. However, the large quantity of liquid lithium required for operation in a steady-state mode should be recognized as the main drawback of the flowing scheme. This means that there will accumulate a large volume of the 'excess' DT fuel of low concentration. This can be a serious problem for DT recovery.

In the FNS on a tokamak basis [25], the energy loads on the wall are reduced and the lithium functions are simplified. The temperature of the chamber walls of such an FNS will not exceed 400 °C. This means that the FNS chamber can be made of SS. Its surface facing the plasma may be protected from direct plasma bombardment by a thin (~3–10 μm) lithium film, which will be created in the course of regular tokamak operation by using an additional lithium source (lithium emitter) placed inside the chamber and into the SOL.

If one places into the SOL additional lithium collectors connected by a lithium MHD pump to an emitter (figure 10), this will allow one to create a closed steady-state loop of lithium circulation near the chamber wall. Thus, lithium will play the role of the erosion product of the PFC and the first wall,

thereby ensuring the existence of a steady-state discharge without an irreversible accumulation of the erosion deposits on the passive areas of the discharge chamber. The noncoronal radiation of lithium ions of such a loop (see appendix A) can play the role of a UV cooler when ions travel through the plasma periphery, which will transfer the heat flux from the plasma column to the entire inner surface of the tokamak chamber (the Sun model) with no additional increase in the wall erosion. Numerical estimates show [43] that, in an FNS with 30 MW of neutron production, the noncoronal UV radiation could transfer to the chamber surface about 20 MW of the total heat flux from the hot plasma by Li injection into the plasma edge at a level of 1 g s^{-1}. This should unload the divertors or limiters of such an FNS.

Figure 10 is a schematic diagram of a closed loop of lithium circulation with D + T separation, which should provide steady-state tokamak operation. In addition to the main aim of a closed loop of lithium circulation, which is to prevent lithium accumulation in the vessel during steady-state tokamak operation, the secondary aim is to decrease the total amount of lithium in the vessel of the tokamak-reactor in accordance with fire and radiation hazards. The straight arrows show the drift of Li ions from the emitter through the SOL up to the collector and the return of the collected lithium atoms back to the emitter in a liquid state. The wavy point arrows denote noncoronal lithium radiation as the cooler of the plasma periphery.

To prevent splashing of the liquid metal from the surfaces of the lithium emitter and collectors during tokamak transient modes, Evtikhin *et al* [50] proposed lithium emitters and collectors in the form of a lithium-filled capillary porous system (CPS). The lithium film on the surface of a capillary solid matrix made of 'tungsten felt' or Mo nets with a cell size of ~10–50 μm can protect it from plasma erosion, as was shown in numerous experiments (e.g. [43, 45–47]). According to the diagram in figure 10, a fraction of the injected lithium will be deposited as a lithium film on the first wall and can protect it from direct plasma bombardment during transient tokamak events, such as ELMs and disruptions. Most of the 'excessive fuel' (D^+ and T^+ ions) captured by the collectors can be extracted from the liquid lithium stream without interruption of tokamak operation by using additional heating in the feedback branch of the circulation loop and then returning it back into the fueling system. Note that steady-state tokamak operation does not require the complete removal of hydrogen isotopes from the liquid lithium. It will be sufficient to substantially reduce their content. The ITER-like version of this diagram is presented in figure 11 [47]. The replaceable vertical lithium CPS limiter with its rod-type geometry, placed in the divertor SOL, plays the role of a lithium emitter. Accordingly, the rod-like divertor targets should play the role of lithium collectors. The arrows show the directions of the drifts of Li ions from the lithium emitter to the collectors.

The rod-type lithium CPS divertor targets and emitters have an important advantage: their 'colder' ends ($T < 300$ °C) can operate in the tokamak SOL as additional collectors of lithium that can return to the 'hot emission spot' ($T > 400$ °C) by capillary forces along the rod [47]. Due to the rod geometry, lithium emitters and collectors can enhance lithium convection and circulation between hot plasma and the chamber, with the additional cooling of the plasma edge by noncoronal lithium UV. The He ash of DT fusion can be removed from the divertor volume of a steady-state FNS by vacuum pumps [47].

For this scheme to operate efficiently it is necessary to know the properties and permissible temperature ranges of each of its elements: the emitter, collectors, and extractors of hydrogen isotopes from the Li stream. These issues were carefully investigated in numerous experiments on the circular ($R/a = 0.7/0.25$ m) tokamak T-11M [47] (appendix B).

The T-11M experiments have led to important practical conclusions about lithium and hydrogen capture by a hot CPS collector filled with liquid lithium. The preferable temperature interval for the efficient capture of lithium ions by a liquid lithium-filled CPS is 200 °C–350 °C, while for the efficient capture of deuterium, it is 200 °C–300 °C. For the efficient removal of deuterium (and probably tritium) from liquid lithium (DT recuperation), heating up to 500 °C–550 °C will be sufficient.

The next important result of T-11M experiments with a heated SS target, which modeled the wall of the FNS chamber, is that the capture of lithium and hydrogen isotopes by films deposited on the target surface in the course of a plasma discharge strongly depends on the temperature of the target. Namely, after the heating of the target to 300 °C–400 °C, the hydrogen capture practically disappears, although the lithium capture decreases only three- to fourfold. Thus, if the first wall of the FNS, permanently protected by a lithium film, is heated to 400 °C, it will play the role of a 'mirror' with respect to the deuterium and tritium ions incident on it. As a result, the total amount of tritium circulating in such a lithium fuel circuit can be reduced to a minimal level. The temperatures indicated by the main elements of the scheme in figure 10 correspond to the recommended temperature ranges of their steady-state operation (appendix B).

The main technical difficulty that will arise in the implementation of such a scheme would be the prevention of poisoning lithium by atmospheric gases, which will inevitably necessitate an additional hermetic shell filled with any noble gas (Ar, in figure 11).

If this technological obstacle is overcome, there will be no physical limitations for the steady-state operation of a closed lithium fuel circuit and, accordingly, no limitations on the duration of the FNS plasma shot, with the exceptions of the current drive problem and the cooling of the discharge chamber.

4. Conclusions

Fifty years ago, shortly before he died, Artsimovich answered the question of when a fusion reactor be will built: 'As soon as anyone will need it.' So, who needs a fusion reactor today or in the next 50 years? First of all, it may be needed as an FNS. The most attractive long-term goal of the current fusion programs in many countries is the creation of a traditional pure fusion (PF) reactor, where fusion energy is obtained without using any actinides in the tokamak blanket. As was mentioned

above, in parallel with this PF strategy, there is another opportunity which looks more attractive and can be realized sooner. It will be based on steady-state preburning tokamaks with DT fusion production at a level of 20–100 MW as commercial FNSs, to meet the needs of existing light water reactor (LWR) energetics.

Firstly, it can be used for waste management by burning the long-lived actinides (transuranics) that are products of LWRs [51]. The transuranics present in the LWR spent fuel are the primary contributors to the waste characteristics, which pose the greatest disposal challenges. The hard neutron spectrum leads to favorable effects for transuranic management in comparison with LWR neutrons [51]. This can be the first step to 'green nuclear energetics'. Secondly, it can be used for the production of LWR fuels (^{233}U, ^{239}Pu) from weakly active and chip ^{238}U and ^{232}Th.

The FNS is a step between laboratory fusion devices and self-sustaining DT reactors with ignition [25]. Prototypes of an FNS could be DT tokamaks similar to TFTR and JET, but operating in the steady or quasi-steady mode.

Obviously, the final opinion on the possible future applications of tokamaks can be obtained only on the basis of the experience of ITER operation in the regime of preburning, and that will be achieved no earlier than in 2030–35. However, some estimates and predictions can be made on the basis of the already available information about the behavior of plasmas in large and small tokamaks [16].

In particular, as could be noted by the reader, this concerns the impact of the parameter P_H/S on the duration of the discharge shot. If one recognizes the validity of the presented analysis, then the path to steady or quasi-steady tokamaks and stellarators as nuclear energy sources is through Li, which plays the role of an intermediate substance between the hot hydrogen plasma and the solid wall. Otherwise, this will be achieved by the less obvious injection of some noble gas into the divertor chamber under the condition of strict control over its penetration into the plasma core. Are there any other, simpler methods? We would like to believe that there are, but we still do not know of them. The lithium method is difficult technologically, but it is not prohibited by the known physical laws. It is based on the exceptional ability of lithium to return almost all captured hydrogen and its isotopes under moderate heating (400 °C–500 °C, Attachment B). It looks to be the 'light at the end of a tunnel'.

Figure 12 presents two TFTR DD discharges [44] with laser injection of lithium aerosol and without it (graphite limiter) as a very impressive sample of using Li in a tokamak. The figure shows the distributions of Z_{eff} along R (major radius) in the TFTR plasma column, with a current of 2.2 MA and neutral injection power of $P_H = 18$ MBт ($P_H/S = 0.23$ MW m^{-2}) [44].

Lithium injection with NB heating made it possible to decrease Z_{eff} in the most important central zone of the plasma column from 2.6 to almost 1, which seems to be the most stringent requirement for all fusion reactors and neutron sources on the basis of a tokamak. The neutron yield in TFTR DD shot #104039 with lithium injection was close to 2.5×10^{16} neutrons per shot. In the case of DT fusion, it should increase by two orders of magnitude, i.e. it will be close to the lower limit of the demands of fission specialists of the power of neutron emission for the first research FNSs [25]. Modern estimates suggest that this limit can be overcome by some optimization of the discharge conditions in a tokamak with parameters like TFTR. It will be substantially more complicated to satisfy the next stringent condition: to switch a tokamak in a steady or quasi-steady mode with a duration of up to several hundred minutes. The future of tokamaks depends on success in this direction.

Acknowledgments

The author thanks I.B. Semenov, A.N. Shcherbak, A.B. Mineev, A.S. Kukushkin and A.S. Sakharov for their assistance.

The work was supported by Russian Science Foundation grant No. 16-19-10457.

Appendix A. Lithium noncoronal radiation [43]

It well known that impurity radiation on the edge of a tokamak plasma column can substantially influence its macroscopic behavior. The effect of its influence is aggravated by the fact that the impurity ions exist at ultimate time τ in the zone between the surface of the chamber and the hot plasma boundary in the SOL, in the area with magnetic lines crossing the wall or limiters (targets). As a result, they are forced to 'travel' between the wall and the plasma, with recombination on the targets and ionization in the SOL plasma.

The radiation of such partially ionized impurities can be several tens of times higher than the calculated value corresponding to the stationary plasma, when the steady-state charge of the impurity will be determined by the equilibrium between electron-impact ionization in the volume of the plasma column and radiative recombination (so-called 'coronal equilibrium' and 'coronal radiation'). By analogy, the ion radiation in a nonequilibrium state is called 'noncoronal'. The noncoronal radiation of Li^+ ions is shown in figure B2 (appendix B) in the form of a green loop stretched along the magnetic field from the vertical lithium emitter of T-11M up to the longitudinal lithium collector. The rate at which the coronal equilibrium of the impurity ions is established depends on the confinement time τ of impurity ions in the SOL and on the plasma density n_e and the electron temperature T_e in the SOL. The product $n_e\tau$ is called the 'nonstationary parameter'.

Figure A1 [43] shows the total radiation power of lithium per single Li atom and per single electron, which was calculated for different electron temperatures (1–1000 eV) and different values of the nonstationary parameter $n_e\tau$ (where n_e is in cm^{-3}, τ is in s, and T_e is in eV; all calculations were carried out by D. Yu. Prokhorov [43] in the coronal approximation). The index 'inf' stands for stationary coronal equilibrium. In the electron temperature range of 30–300 eV, the power of noncoronal lithium radiation can exceed the equilibrium coronal limit by two to three orders of magnitude.

To estimate the SOL cooling effect by lithium ionization and radiation, we can use the so-called 'energy cost of atom

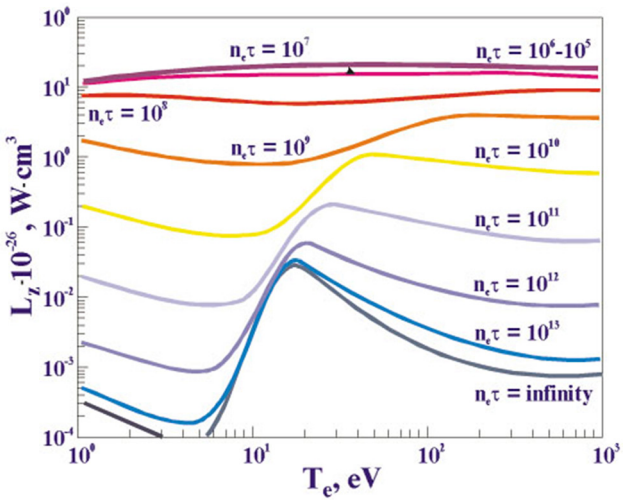

Figure A1. Total radiation power of lithium per single Li atom and per single electron. Adapted from [43]. © IOP Publishing Ltd. All rights reserved.

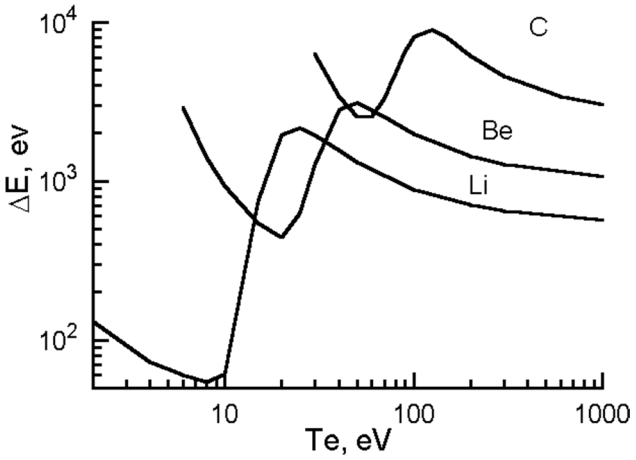

Figure A2. 'Ion energy cost' as a function of the electron temperature in the tokamak SOL for Li, Be, and C. Adapted from [43]. © IOP Publishing Ltd. All rights reserved.

ionization', which is the total electron energy loss during a transition of one neutral atom into the coronal ionization balance. Figure A2 shows the 'energy costs of atom ionization' of Li, Be, and C atoms as functions of the electron temperature. We can see that lithium is a more efficient coolant of the plasma in the range $T_e = 13$–30 eV in comparison, for example, with beryllium. The experiments carried out on the T-11M and T-10 tokamaks show that the actual 'energy costs of Li atom ionization' at the plasma periphery are close to 1 keV.

Appendix B. T-11M experiment [43, 47, 52]

The main parameters of the T-11M tokamak are as follows: $R = 0.7$ m, $a = 0.2$ m, $B_T = 1.2$ T, plasma current $J_p \approx 100$ kA, shot duration $\Delta t = 0.15$–0.25 s, $n_e = (1$–$6) \times 10^{19}$ m^{-3}, $T_e(0) = 400$ eV, $n_e(\mathrm{SOL}) = (2$–$5) \times 10^{18}$ m^{-3}, and $T_e(\mathrm{SOL}) = 5$–30 eV [45]. The main aim of the T-11M group activity [45, 49] was to find out the permissible temperature intervals of operation for each Li loop element: the emitter,

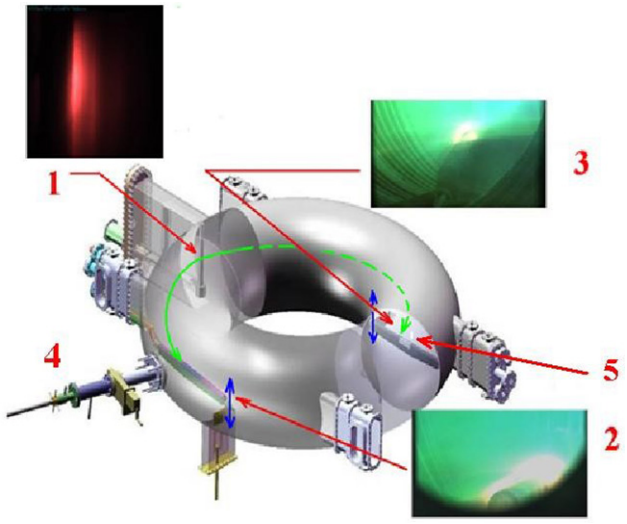

Figure B1. Diagram of the T-11M: (1) lithium CPS emitter; (2, 3) two longitudinal (tangential to B_T) lithium collectors, and; (4) movable SS target. Arrow 5 is the FOV of the video and UR cameras of longitudinal collector 3.

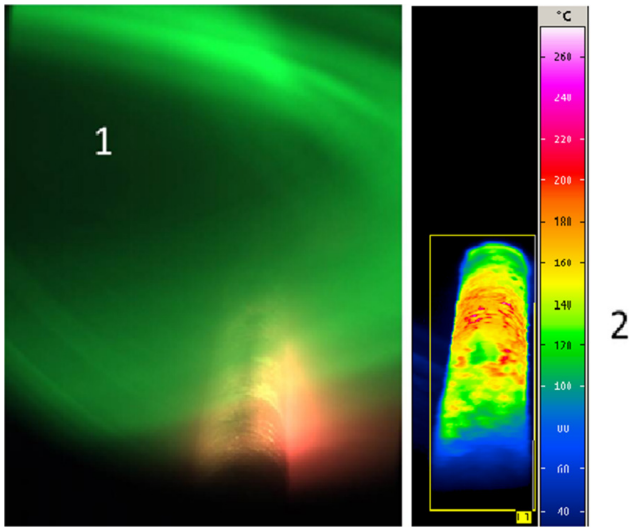

Figure B2. View of the longitudinal limiter-collector of T-11M in visible (1) and infrared (2) light during plasma shot. The right panel shows a view of the longitudinal CPS collector in the infrared light. One can see the localization of 'warm' (200 °C–220 °C) and 'cold' areas (<100 °C) of the active lithium and hydrogen collection.

collectors, and extractors of hydrogen isotopes from the Li stream.

The diagram of T-11M (figure B1) shows the main elements of the FNS lithium loop, which was presented above: (1) a vertical rod-type lithium CPS emitter as the main tokamak limiter, and; (2, 3) two longitudinal (tangential to B_T) rod-type CPS limiters used as two lithium collectors. Movable SS target 4 was used to study lithium accommodation on the FNS first wall and the capture of hydrogen isotopes by the deposited lithium. Arrow 5 is the field of view (FOV) of video and UR cameras of longitudinal lithium collector 3.

Figure B2 presents a view (FOV 5) of the longitudinal lithium CPS collector recorded in a plasma shot by color (1) and infrared (2) video cameras. The localization of the

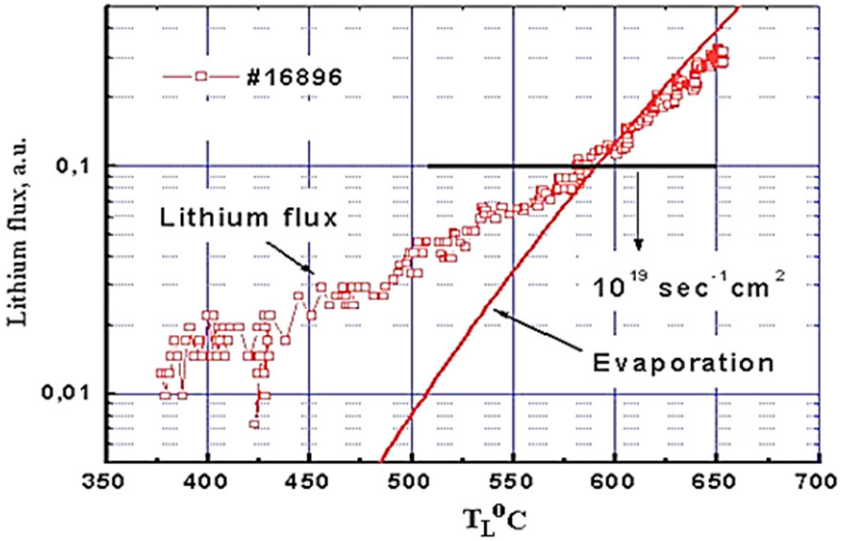

Figure B3. Measured and calculated fluxes of neutral lithium versus emitter surface temperature T_L in the active phase of T-11M shot #16896 [43]. Adapted from [43].

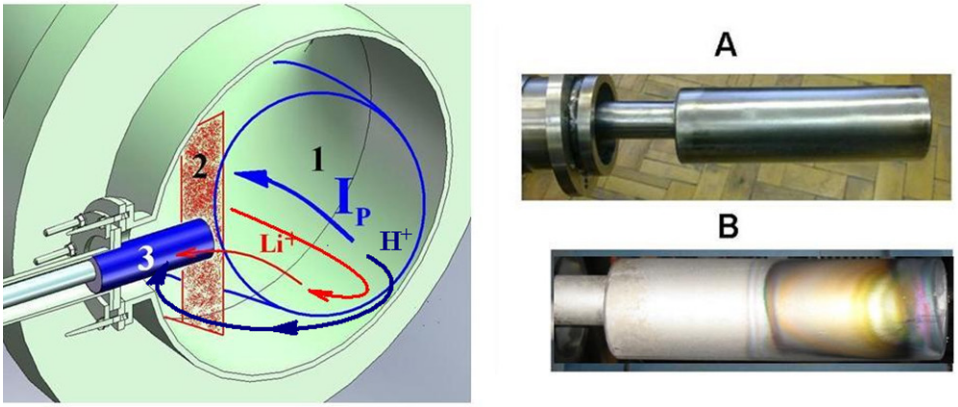

Figure B4. On the left: cryogenic target in T-11M: (1) plasma, (2) vertical limiter, (3) target. On the right: (*A*) view of the target head before lithium collection, and; (*B*) after the collection experiment, with Li_3N film clear to see on its surface.

areas of neutral lithium collection (recombination light) is shown in red, while green shows the spatial distribution of Li^+ streams from the vertical emitter (it is placed on the left) along the total magnetic field with the bright lithium noncoronal radiation.

B.1. Permissible temperature range of the Li CPS emitter

The Li CPS emitter of T-11M (figure B1, item 1) operated as a vertical tokamak limiter with an auxiliary heater. The temperature of the limiter surface during a discharge varied from 50 °C to 750 °C. The neutral lithium line (607.8 nm) emission near the limiter surface was used to estimate the lithium flux. The typical thermal load on the Li CPS surface was about 10 MW m^{-2} in normal discharges and reached 100–200 MW m^{-2} during disruptions [41]. No catastrophic events leading to spontaneous lithium injection in the lithium temperature range (from 20 °C to 600 °C) were observed. As the Li temperature increased up to 650 °C, bursts of lithium emission and visible oscillations of the limiter surface temperature were detected [43]. This means that we can choose 700 °C as the upper operation limit for the Li emitter in a steady-state tokamak.

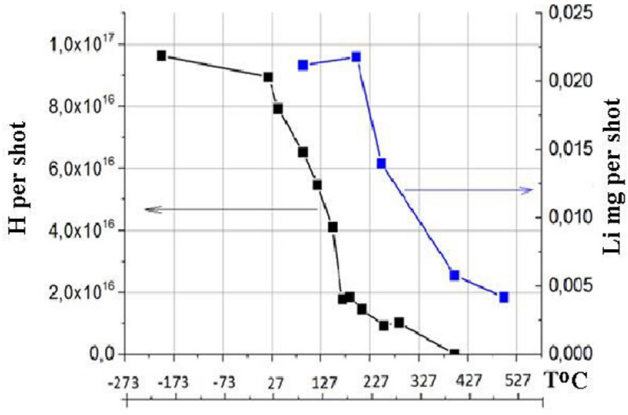

Figure B5. Amount of lithium and hydrogen captured by a metal target per shot as a function of the target temperature *T*.

Figure B3 shows the lithium influx measured in T-11M shot #16869 as a function of the emitter surface temperature T_L. Obviously, the main mechanism of Li emission in

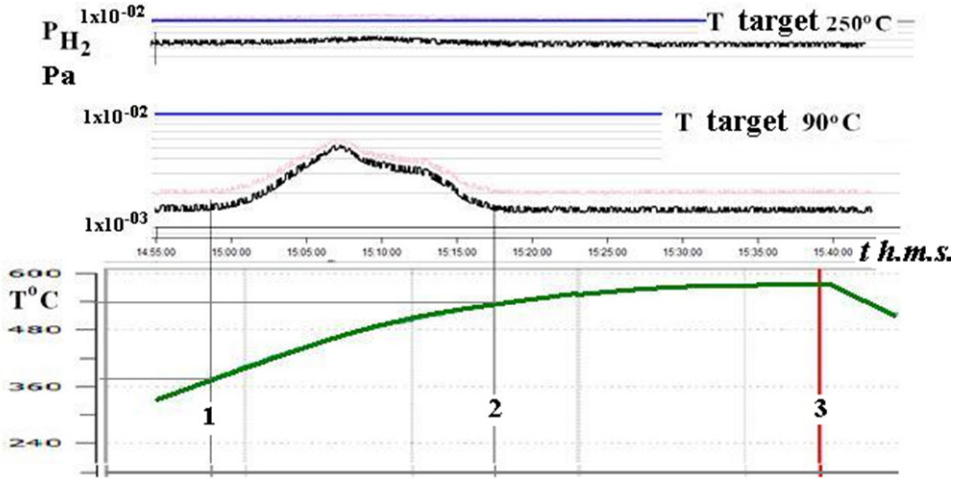

Figure B6. TDS spectra of hydrogen for two target exposures in plasma discharge at 90 °C and 250 °C and heating dynamics $T(t)$.

the temperature range of 300 °C − 500 °C is the erosion of liquid Li during plasma bombardment. For emitter temperatures higher than $T_L \approx 500$ °C, Li evaporation is the main mechanism of lithium emission, which increases nearly exponentially with increasing T_L. Experiments with preliminary saturation of the lithium surface of the emitter by a glow hydrogen discharge have shown a moderate (no more than 20%) decrease in lithium emission [53].

B.2. Permissible temperature ranges of the FNS first wall and Li CPS collectors

A massive ($D = 60$ mm) SS target in the form of a thin-walled cylinder was inserted into the SOL of the plasma column of the T-11M tokamak in order to simulate the process of accumulation of lithium and hydrogen by the first wall during a lithium experiment. The target (figure B1, item 4) was introduced into the chamber through a vacuum lock, which allowed one to insert the target in the chamber or remove it between plasma shots without a vacuum break. The cylindrical surface of the target could be cooled from the inside to the temperature of liquid nitrogen, or heated up to 600 °C. The target was removed from the tokamak chamber after plasma exposure in a series of plasma shots with the aim of determining the amount of the captured lithium. Figure B4 is a scheme of the experiment, as well as the view of the target before exposure in a T-11M plasma discharge and after it.

The absolute amount of lithium accumulated in the form of films on the surface of the cylinder (~200 cm^2) during exposure was measured by the method of 'dissolution in hot water' [54], followed by analysis of the LiOH content by chemical and spectroscopic methods (flame atomic emission spectrometry (FAES)). The total time of each exposure in the plasma discharge was usually about 5 s, which corresponded to 30 shots of T-11M tokamak with durations of about 0.2 s each. The absolute number of hydrogen (or deuterium) atoms captured by lithium during such exposures was measured by a residual gas analyzer (RGA) by using thermal desorption spectroscopy (TDS) of the accumulated lithium films by heating the target in the tokamak vacuum chamber from the initial temperature T_0 to 550 °C–600 °C.

The results of such analysis are presented in figure B5. It was found that the capture of lithium by a metal target in the SOL remains nearly constant with increasing target temperature T_0 from −200 °C to 200 °C and then gradually decreases about five- to six-fold as T_0 increases to 300 °C–400 °C. The capture of hydrogen by a steel target behaves similarly to lithium in the temperature range of −200 °C to 100 °C, but then decreases almost 100 times as the temperature increases to 300 °C–400 °C. It was found that deuterium behaves like hydrogen.

Thus, it should be expected that if the temperature of the steel wall of the vacuum chamber of the FNS reaches 300 °C–400 °C, a thin layer of lithium (or its chemical compounds) coating on the inner wall of the chamber should play the role of a 'mirror' for the flows of deuterium and tritium falling from the plasma SOL. Thereby, the heating of the steel vacuum chamber up to $T_0 > 300$ °C–400 °C should minimize the accumulation of tritium by the inner wall of the vacuum chamber up to the lowest values during steady (quasi-steady) operation.

Similar experiments with the replacement of a steel target with a Li CPS collector (figure B1, item 2) showed that the capture of deuterium by the liquid lithium surface of the CPS remains efficient up to 250 °C–300 °C. In parallel, the flux of Li ions from the SOL is efficiently captured by the Li CPS collector up to 350 °C. Thus, the capture of 'excess' lithium and fuel (DT) by the limiters or divertor collectors on the basis of a liquid Li CPS is possible in the temperature range of 200 °C–300 °C. Then, the captured deuterium and tritium can be transferred from the collector to the recovery zone by the flow of liquid lithium.

The characteristic heating temperature required for their recovery can be determined from the results of TDS of lithium films on the surface of an SS target. Figure B6 shows TDS spectra of hydrogen for two target exposures in the plasma discharge at 90 °C and 250 °C and those obtained by heating to 550 °C (lower curve, position 3). One can see that active hydrogen desorption begins at the target temperature of 370 °C (position 1) and finishes at 500 °C (position 2). The

recommended operating temperatures of various circuit elements are shown in figure 10.

References

[1] Gorbunov E.P. and Pazumova K.A. 1963 *At. Energy* **15** 363
[2] Artsimovich L.A., Mirnov S.V. and Strelkov V.S. 1964 *At. Energy* **17** 170
[3] Grigorovich B.M. and Mukhovatov V.S. 1964 *At. Energy* **17** 177
[4] Mukhovatov V.S. and Shafranov V.D. 1971 *Nucl. Fusion* **11** 605
[5] Vinogradova N.D. and Razumova K.A. 1965 *Plasma Physics and Controlled Nuclear Fusion Research (Proc. 2nd Int. Conf. Culham 1965)* (Vienna: IAEA) 1966, v II, p 617
[6] Mirnov S.V. and Semenov I.B. 1971 *JETP* **33** 1134
[7] Mirnov S.V. 1969 *Nucl. Fusion* **9** 57
[8] Gorelik L.L. *et al* 1970 *Nucl. Fusion* **12** 185
[9] Gorbunov E.P., Mirnov S.V. and Parfenov D.S. 1971 *Nucl. Fusion* **11** 433
[10] Bobrovskii G.A. and Razumova K.A. 1971 *JETP Lett.* **14** 99
[11] Artsimovich L.A. *et al* 1968 *Plasma Physics and Controlled Nuclear Fusion Research (Proc. 3th Int. Conf. Novosibirsk 1968)* (1969) (Vienna: IAEA) vol I, p 157
[12] Artsimovich L.A. 1972 *Nucl. Fusion* **12** 215
[13] Artsimovich L.A. *et al* 1971 *Plasma Physics Controlled Nuclear Fusion Reserach (Proc.4th Int. Conf. Madison)* (Vienna: IAEA) 1971 vol 1, p 443
[14] Gorbunov E.P., Mirnov S.V. and Strelkov V.S. 1970 *Nucl. Fusion* **10** 43
[15] Kadomtsev B.B. 1978 *Nucl. Fusion* **18** 553
[16] ITER Physics Expert Groups 1999 ITER Physics basis *Nucl. Fusion* **39** N12
[17] Kadomtsev B.B. and Pogutse O.P. 1978 *Plasma Phys.and Contr. Nucl. Fusion Res. (Proc.7th Int.Conf. Insbruk)* (Vienna: IAEA) (1979) vol 1, pp 649–63
[18] Callen J.D. 1977 *Phys. Rev. Lett.* **39** 1540
[19] McGuire K.M. *et al* 1995 *Phys. Plasmas* **2** 2176
[20] Artsimovich L.A. and Shafranov V.D. 1972 *JETP Lett.* **15** 72
[21] Vorobiev A.V. *et al* 1978 *Fyz. Plasma* **4** 982
[22] Eubank H. *et al* 1978 *Plasma Phys. and Contr. Nucl. Fusion Res. (Proc.7th Int. Conf. Insbruk)* (Vienna: IAEA) 1979 vol 1, pp 167–98
[23] Murakami M., Callen J.D. and Berry L.A. 1976 *Nucl. Fusion* **16** 347
[24] Greenwald M. *et al* 1988 *Nucl. Fusion* **28** 2199
[25] Mirnov S.V. 2013 *Plasma Phys. Control. Fusion* **55** 045003
[26] Strachan J.D. *et al* 1994 *Phys. Rev. Lett.* **72** 3526
[27] Hawryluk R.J. *et al* 1998 *Phys. Plasmas* **5** 1577
[28] Ishida S. *et al* 1996 *16 IAEA Fusion Energy Conf. (Montreal, Canada)* (Vienna: IAEA) vol 1, p 315
[29] JET Team (presented by M Keilhacker) 1997 *Plasma Phys. Control. Fusion* **41** B1
[30] Neu R. *et al* 2012 *PSI-20 Aachen I-2*
[31] Marmar E. *et al* 2006 *21 IAEA Fusion Energy Conf. (Chengdu, China)* p EX/3-4 (www-naweb.iaea.org/napc/physics/FEC/FEC2006/html/index.htm)
[32] Greenfield C.M. and the DIII-D Team 2010 *23 IAEA Fusion Energy Conf. (Daejeon, Rep. Korea)* OV/14 (www-naweb.iaea.org/napc/physics/FEC/FEC2010/html/index.htm)
[33] Vershkov V.A. *et al* 2014 *25 IAEA Fusion Energy Conf. (St. Petersburg RF)* p EX/11-2Rb (www-naweb.iaea.org/napc/physics/FEC/FEC2014/html/index.htm)
[34] Dumont R. *et al* 2012 *39th EPS Conf. on Plasma Physics and Controlled Fusion (Stockholm, Sweden)* p P4.005 (http://ocs.ciemat.es/epsicpp2012pap/html)
[35] DOE 2012 *Fusion Energy Sci. Com. Rep.* DOE/SC-0150 Fig. 4.02
[36] Zushi H. *et al* 2005 *Nucl. Fusion* **45** S142
[37] Oh Y.-K. *et al* 2016 *Preprint: 2016 IAEA Fusion Energy Conf. (Kyoto, Japan)* p OV/2-4 (www-naweb.iaea.org/napc/physics/FEC/FEC2016/html/index.htm)
[38] Wan B.N. *et al* 2017 *Nucl. Fusion* **57** 102019
[39] Mirnov S.V. 2016 *Plasma Phys. Control. Fusion* **58** 022001
[40] Wesson J. 2004 *'Tokamaks' 3/e* (Oxford: Oxford University Press) p 473
[41] Peter W. *et al* 1983 *IAEE Trans. Nucl. Sci.* **30** 3454
[42] Evtikhin V.A. *et al* 2002 *Plasma Phys. Control. Fusion* **44** 955
[43] Mirnov S.V. *et al* 2006 *Plasma Phys. Control. Fusion* **48** 821
[44] Mansfield D.K. *et al* 2001 *Nucl. Fusion* **41** 1823
[45] Apicella M.L. *et al* 2005 *Fusion Eng. Des.* **75–79** 351
[46] Vershkov V.A. *et al* 2017 *Nucl. Fusion* **57** 102017
[47] Mirnov S.V. *et al* 2015 *Nucl. Fusion* **55** 123015
[48] Ono M. *et al* 2016 *Preprint: 2016 IAEA Fusion Energy Conf. (Kyoto, Japan)* p FIP/2-5 (www-naweb.iaea.org/napc/physics/FEC/FEC2016/html/index.htm)
[49] Hu J.S. *et al* 2016 *Nucl. Fusion* **56** 046011
[50] Evtikhin V.A. *et al* 1996 *16 IAEA Fusion Energy Conf. (Montreal, Canada)* (Vienna: IAEA) 3 p 659
[51] U.S. DOE 2009 *'Fission Fusion' Rep. of Res. Needs Workshop (ReNeW) (Gaithersburg, MD, 30 September–2 October 2009)* ch 3, p 30
[52] Shcherbak A.N. 2017 *44th EPS Conf. on Plasma Physics (Belfast)* p P5.112
[53] Mirnov S.V. *et al* 2013 *J. Nucl. Mater.* **438** S224–8
[54] Azizov E.A. *et al* 2009 *36 EPS Conf. on Plasma Physics and Controlled Fusion (Sofia, Bulgaria)* p P5.192 (http://epsppd.epfl.ch/Sofia/html/preface.htm)